Contents lists available at ScienceDirect

Precision Engineering

journal homepage: www.elsevier.com/locate/precision





Preliminary study of photomask pattern inspection by beam-shaped knife-edge interferometry

Zhikun Wang, Pengfei Lin, ChaBum Lee

J. Mike Walker '66 Department of Mechanical Engineering, Texas A&M University 3123 TAMU, College Station, TX 77843, 3123, USA

ARTICLE INFO

Keywords:
Photomask inspection
Knife-edge interferometry
Critical dimension
Line-edge quality
Interferogram analysis

ABSTRACT

This paper presents a photomask inspection and defect analysis technique to accurately measure the pattern dimensions and to detect the defects of the photomask in a convenient, fast, reliable manner. The beam-shaped knife-edge interferometry (BSKEI) was developed to collect the interferogram created by the superposition of the reference incident wave and the edge-diffracted wave while scanning the photomask. BSKEI consists of a pulsed laser diode, an aperture, an objective lens, and a fiber-coupled photodiode. The objective lens enabled the beam shaping to create a spherical wave as a new source of light, and the beam shaping was effective to enhance the spatial frequency of the interferogram. The interferograms were characterized based on a Fresnel number model, and the corresponding interferogram analysis methods were developed. BSKEI produced different interferograms according to the photomask patterns and defects while scanning the photomask. As a result, BSKEI is capable of the measurement of pattern width, opening width, line-edge quality, and opening area surface quality of the photomask, and is expected to be an alternative tool for critical dimension metrology in many semiconductor applications.

1. Introduction

A photomask inspection and metrology assuring their quality or conditions is a key technology in lithography to achieve semiconductor device manufacturing with high reliability and high yield. A photomask is an opaque glass substrate with patterned structures and an opening area. Because the mask patterns are projected onto the silicon or other substrates, quality control of the photomask is critical for precise, defect-free pattern generation [1,2]. Many semiconductor industries have been automating the photomask inspection and metrology involving scanning electron microscopy (SEM) or other existing advanced measurement systems, and eagerly require new technology for fabricating, inspecting, quality controlling, and repairing photomasks with high accuracy and high resolution [3–5].

The defects of the photomasks can be defined as unwanted or damaged patterns. For instance, the pattern dimension could be smaller or larger than designed, and the line-edge roughness (LER) of the patterns has a significant impact on printability due to light scattering at the edge [6–8]. The images projected from the defected photomask may have distortion, and the fabricated device may alter the electrical or material properties of what was being fabricated [3,4]. Some defects

could be induced from the glass substrate manufacturing processes, photomask writing processes, etching processes, developing processes, or baking processes, and sometimes photomasks could be damaged during the photolithography processes [9].

Therefore, advanced photomask inspection metrology enabling defect analysis and printability simulation are essential to assess the critical dimension lithography performance [10]. However, current methods such as SEM or "Nightmare" photomask testing are inconvenient and expensive and are limited to in-process inspection. The effective photomask inspection technology is in high demand because it enables high accuracy and high-resolution lithography printability and increases in photomask cycle times.

The semiconductor manufacturers have introduced advanced photomask inspection systems, data analysis software, learning-based defect identification algorithms, and printability prediction models since 2000. With the advent of extreme ultraviolet (EUV) lithography enabling high volume manufacturing, semiconductor manufacturers need more advanced photomask inspection technology. Kim et al. utilized images from a high-resolution mask inspection system combined with the transmitted and reflected images, and then developed the mask recovery process and modeling method that allows flexibility to

E-mail address: cblee@tamu.edu (C. Lee).

^{*} Corresponding author.

simulate the lithography printability [11]. Oh et al. introduced a photomask defect detection and inspection method by using aerial imaging and high-resolution imaging [12]. Rajendran addressed the technological gap in several defect inspection methods available at several industries [13]. Penley et al. studied haze formation by using mass spectroscopy and atomic force microscopy and the resultant pellicle degradation and reported the chemical mechanism of developing defect generation and growth on the photomask [14]. Many advanced technologies for photomask defect inspection and metrology have been introduced, but those systems are developed for the manufacturers' internal use, so there are few commercial products available in the market.

Lee et al. previously developed knife-edge interferometry (KEI) and applied this method for cutting tool inspection, sharp-edge corrosive wear propagation, and displacement measurements [15–18]. In this study, the performance of KEI was significantly enhanced by implementing the beam shaping method, and the beam-shaped knife-edge interferometry (BSKEI) was newly introduced. The optical model to simulate the interferogram was discussed to increase the performance of photomask inspection.

2. Measurement principle

2.1. Beam-shaped knife-edge interferometry

The principle of the BSKEI as illustrated in Fig. 1 can be explained by the theory of geometrical optics. Here, the pattern width (P), pattern distance (D), LER, and arbitrary defects (e.g., air voids, scratches, residual photoresist, or dust) on the photomask will be characterized. Unlike the conventional KEI [15–18], the BSKEI uses an objective lens to shape the collimated beam, and a spherical wave as a new light source incidents on the pattern edges. The objective lens focuses the incident beam on the focal point, and the spherical wave diverges along the light propagation direction. Here, the beam at the focal point can be assumed to be a point source. In those circumstances, all the light at the plane of the sharp edge can be viewed as the secondary wavelet emitted from that plane. The interferogram can be created by the superposition of the reference incident spherical wave and the edge-diffracted wave while scanning the photomask. Such diffraction phenomenon can be characterized by using a Fresnel (F) number model [19] in Eq. (1). In this model, the F-number means the amounts of half-period zones in the plane. Each zone implies the constructive and destructive light intensity effects on the on-axis observation point.

$$F = \frac{\alpha^2}{\lambda \times Z_{reg}} \tag{1}$$

where α indicates the beam radius of the laser at the edge plane, λ is the wavelength of the laser, and Z_{eff} is the effective distance related to the Z_{src} and Z_o . The Z_{src} shows the distance between the focal point of objective lens and the edge plane, while Z_o indicates the distance from the edge plane to the detector. Here among Z_{eff} can be expressed as a function of Z_{src} and Z_o as:

$$\frac{1}{Z_{\rm eff}} = \frac{1}{Z_{\rm NC}} + \frac{1}{Z_{\rm o}} \tag{2}$$

When the Z_0 is 100 times larger than Z_{src} , the Z_{eff} is approximately equal to Z_{src} . Equation (1) can be modified by using a numerical aperture (NA) of the objective lens as follows,

$$F = \frac{NA^2 \times Z_{src}}{\lambda} \tag{3}$$

The edge diffraction simulation provides the output intensity of the on-axis point on the detector plane. In the conventional KEI system, the light fully transmits to the detector with a size of a few hundred micrometers. The intensity of those off-axis points decreases the sensitivity

of the recorded data and generates the attenuated fringe pattern due to the averaging effect by the large detector effective area. However, in the BSKEI system, the incident beam is shaped by the objective lens, and then, the spherical wave incidents on the photomask. Here, interferogram can be generated by the superposition of the reference incident spherical wave and the edge-diffracted wave. Only a small amount of the light is recorded because of the light scattering at the edge. Thus, the averaging effect by the detector effective area can be minimized, and the spatial resolution of the interferogram can be improved. This improvement can be also explained from Eq. (2). It shows that the F-number increases as the NA increases, so the number of fringe patterns increases by shaping the beam by using the objective lens. The measurement details are schematically illustrated in Fig. 1.

2.2. Feature extraction and selection for defect classification

Conventionally, the cross-correlation-based method was used for the KEI fringe analysis (15–17). In this research, the wavelet-based feature extraction method was also studied to improve the defect case analysis performance. The wavelet-based feature extraction method is closely related to the wavelet signal decomposition. After performing the decomposition of the raw data in a multi-scale manner using multiple filters, the coefficients of each resulting component can be classified as the extracted features that contain important time-frequency information of the raw data [20,21]. After the extraction process, a feature selection is then performed to find the feature with the best discrimination ability. In the simulation process, the wavelet-based feature extraction method was applied to analyze the interferograms generated from the BSKEI model. The simulated data consists of 2 groups:

- (1) Group A: 5 simulated fringe patterns with different phase lags shown in Fig. 2. Their phase delays were set to 0 μ m, 15 μ m, 30 μ m, 45 μ m, and 60 μ m, respectively. They were used to simulate the results obtained from the pattern structures with different widths.
- (2) Group B: 5 simulated fringe patterns with different damping levels shown in Fig. 3. The damping was added by multiplying the exponential term with the original fringe pattern. They shared similar patterns with measurement results from the pattern structures with different roughness.

From the simulation result in Fig. 3d, the setup of a conventional KEI system with a $10 \times$ objective lens is sensitive to the damping ratio changes. Here the damping can present the amplitude decrease due to the change in edge roughness [15]. The relative value changes more than 35% in case of the simulated data of BSKEI with $10 \times$ objective lens. On the other hands, the other two conditions shows less than 5% relative value difference. These simulation results showed that the wavelet analysis method for edge roughness characterization is effective because the damping of the fringe pattern is directly related to the edge roughness of the pattern structures.

3. Experiments

As illustrated in Fig. 1, a collimated laser (λ 532 nm) propagates through a 1.0 mm aperture, and then, is focused by an objective lens. A photomask with two straight-line patterns was securely fixed on the precision linear stage. A scanning speed was set to 1 mm/s. For two straight-line patterns, Line #1 and Line #2 are the experiment and the control groups, respectively. The fiber pigtailed avalanche photodiode (APD) was placed at the detector plain. The $Z_{\rm src}$ and $Z_{\rm o}$ were set to approximately 70 µm and 120 mm, respectively. While linearly scanning the photomask, the output voltage of APD was recorded by the National Instrument (NI) data acquisition board. In the experiment, the photomask patterns were scanned twice under the same scanning conditions. First, the whole photomask line pattern with no defect was tested for

Fig. 1. Principle of beam-shaped knife-edge interferometry for photomask inspection.

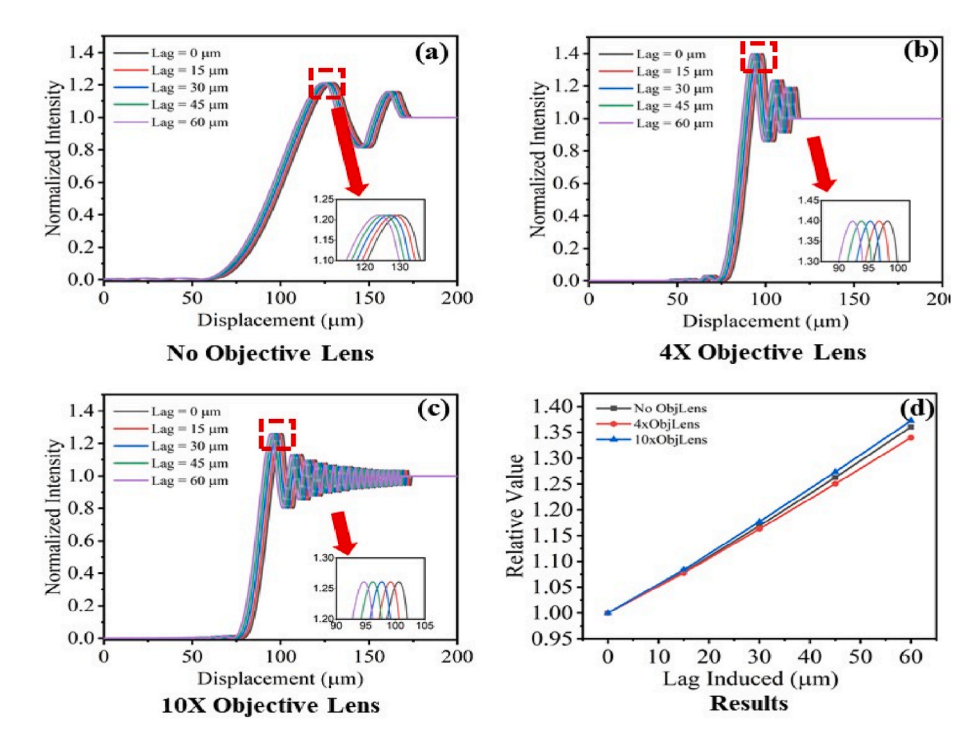


Fig. 2. The simulated lag of fringe pattern analyzed by wavelet method. (a) lag added for fringe pattern in no objective lens case, (b) lag added for fringe pattern in 4 × objective lens case, (c) lag added for fringe pattern in 10 × objective lens case, and (d) results of lag analyzed by wavelet method.

reference, which was recorded as Test #1. After that, the photomask with the defects that were artificially added was scanned for the experiment group, Line #1. Once the defect was added, the experiment was repeated. This time the data was recorded as Test #2. The Line #2 in the pattern was also tested as the control group. After that, the cross-correlation method and the wavelet-based feature extraction method were used to analyze the fringe patterns obtained in two sets of the measurements: Test #1 and Test #2. Based on the result, the photomask pattern parameters (P, D, LER, and defects) could be precisely measured and characterized. During the experiment, a microscope was used to image the photomask profile and conditions for validation.

4. Results

The photomasks were prepared and were scanned by the BSKEI. There were two types of the photomasks to be tested. In the photomask #1, there are two opening areas with pattern width 1.0 mm and other area is Cr-coated. On the other hands, the photomask #2 has two Cr coated patterns with the pattern width 0.5 mm, and other area is transparent. Each sample has two identical patterns, and those patterns were scanned in two cases: without defect (control group) and with defect (experiment group). Here the defect was added to only one of the

two identical patterns in the experiment group. Experiment results for the photomask #1 with 1.0 mm width opening area) can be seen in Fig. 2. The results of 1.0 mm width line photomask pattern measurements indicated:

- (1) The width of the line pattern can be measured precisely. The result of width measurement can be found in Fig. 1f. The actual data and the difference between the actual data and measured data were shown in Table 1. In the measurement, the differences of line width are 0.33% and 0.69%, respectively for the experiment group and control group in the Test #1. In the Test #2 the difference of line width was similar to the case of Test #1.
- (2) The line interval can also be measured. Based on the information from Fig. 4a and c, the distance between the right edge of Line #1 and the left edge of Line #2 is 2.9921 mm from Fig. 4a and 2.9962 mm from Fig. 4c.
- (3) The LER can be determined by using the cross-correlation method to analyze the similarity for each group during the experiment. In this experiment, the defect was added in the Line #1. An additional thin film layer was artificially attached to represent the defect at the pattern edge. The additional film layer changes the width of the opening area pattern, and could play as a Cr layer. It

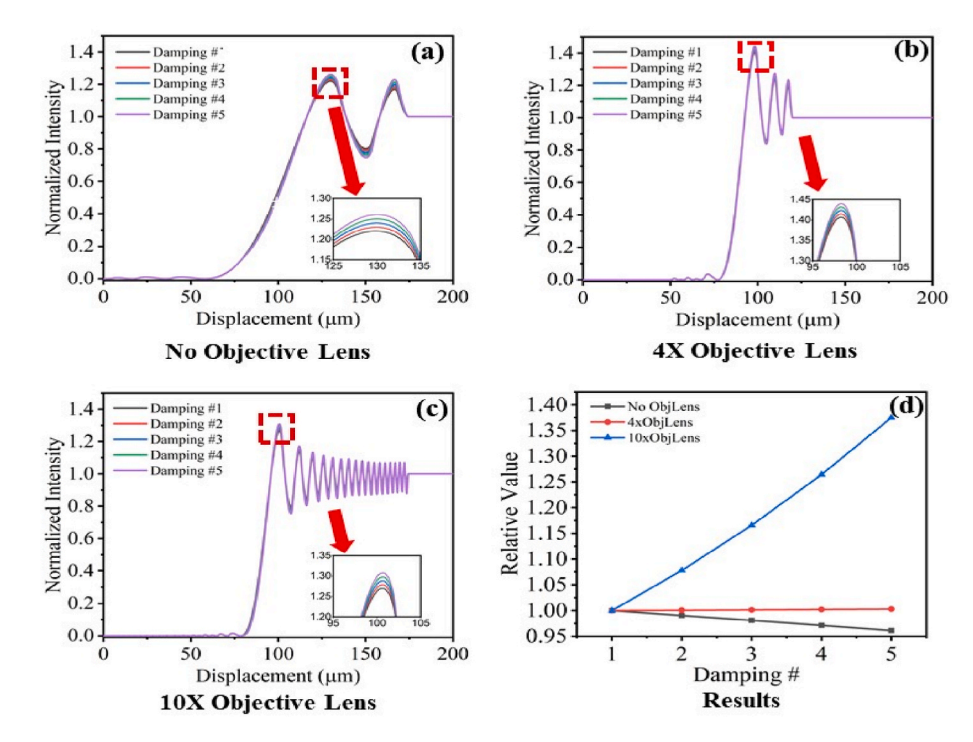


Fig. 3. The simulated damping of fringe pattern analyzed by wavelet method: (a) damping added for fringe pattern in no objective lens case, (b) damping added for fringe pattern in 4×0 objective lens case, (c) damping added for fringe pattern in 10×0 objective lens case, and (d) results of damping analyzed by the wavelet method.

 Table 1

 Line width measurement result of the photomask #1.

	Test	experiment group	experiment group (microscope validation)	control group	control group (microscope validation)
-	# 1	994.5 μm	997.8 μm	996.5 μm	1002.2 μm
	# 2	667.6 μm	667.5 μm	994.0 μm	1002.2 μm

 Table 2

 Line width measurement result of the photomask #2.

•	Test	experiment group	experiment group (microscope validation)	control group	control group (microscope validation)	
	# 1	500.5 μm	501.1 μm	499.9 μm	498.9 μm	
	# 2	1091.5 μm	1094.1 um	501.3 um	498.9 um	

was observed that the edge of the additional film layer is not as sharp as the photomask pattern edge. The Line #1 with the defect added can be seen in Fig. 4c. On the top, the small picture in that diagram shows how the Line #1 was damaged by adding additional film layer. Due to the rough edge of the additional film layer, the left side fringe pattern for Line #1 in Test #2 attenuated radically compared with the result in Test #1. This attenuating fringe pattern also caused the similarity to decrease from 1 to 0.907, while the similarity for the control group only decreases from 1 to 0.9866. The reason for the decrease in the similarity in the control group could be because of DC power switching noise, data acquisition error, dust on the photomask, etc. The fringe patterns for those two groups in the experiment can be found in Fig. 4b and d.

The photomask #2 has two identical Cr patterns with 500 μ m width, and other area is transparent. In the same way, this photomask was scanned by BSKEI. In this experiment, an additional film layer was attached on the Line #1 to add defects. The Line #1 is the experiment

group, and the Line #2 is the control group. Results for the 500 μm width Cr line pattern can be seen in Fig. 5. The results indicated:

- (1) Even though the laser has $\phi 1$ mm beam width, BSKEI measured patterns with a size less than its beam width. The width measurement shows good consistency with the microscope validation. The line width measurement results for 500 μm width Cr line patterns can be found in Table 2. In the result, the difference in width measurement was only 0.47%. In this experiment, the additional film layer increased the width for the Cr coated area because the film layer played as a Cr coating pattern. The measurement results showed good agreement with it.
- (2) The line interval can also be measured. From Fig. 5a, the distance from the left-side edge of Line #1 to the right-side edge of Line #2 was 1.4981 mm, while the measurement result for that distance in Fig. 3c was 1.4933 mm. These two measurement results show good agreement with each other.
- (3) In this experiment, the left edge of the additional film layer was cut directly by a sharp razor blade. So, the edge roughness seldom changes. Even though the defect was added to the photomask, the similarity of the left edge for the experiment group just decreases from 1 to 0.9933, while the similarity for the edge in the control group decreases from 1 to 0.9909. This similarity decay can be explained by the uncertainty of the experiment. This result proved that the BSKEI improves the performance of edge roughness characterization compared with the conventional KEI. The fringe pattern and similarity result can be found in Fig. 5b and d.
- (4) In Fig. 4a, c, 5a, and 5c, when the light passes through the opening area of the photomask pattern, ideally the recorded light intensity should be in a constant value. But in the experiment, the fluctuation of light intensity was observed. It might result from the irregularity of the glass surface. During the manufacturing process of the photomask, the glass plate was coated with the metal layer. These processes could slightly change the thickness or reflectance of the photomask in a certain amount of small area, thus affect the reflectance and attenuation rate of the glass plate.

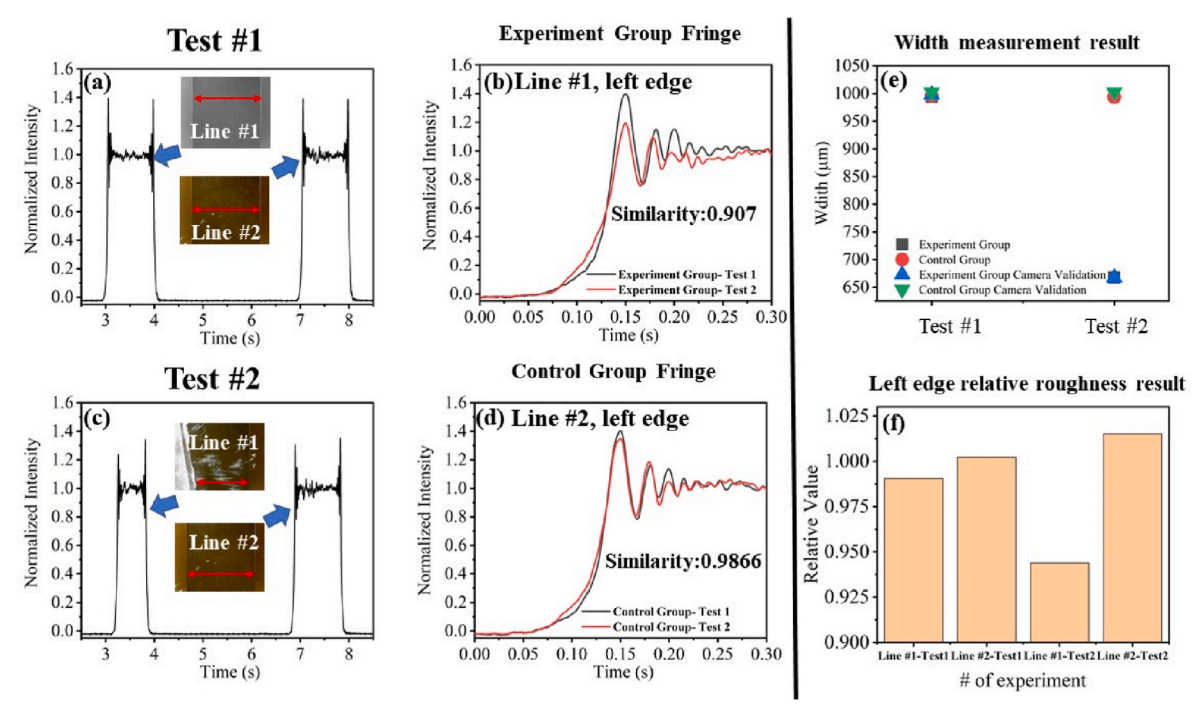


Fig. 4. Photomask #1 scanning results: (a) the scanning results of Test #1 (Line #1 and Line #2 were labeled in the graph with a real-time photo of those two-line patterns from the 10 0× microscope), (b) the fringe pattern for the experiment group in Test #1 and Test #2, (c) the scanning results of Test #2, (d) the fringe pattern for the control group in Test #1 and Test #2, (e) line width measurement result from the BSKEI method and validation by using an optical microscope, and (f) line edge roughness estimated by using the wavelet method.

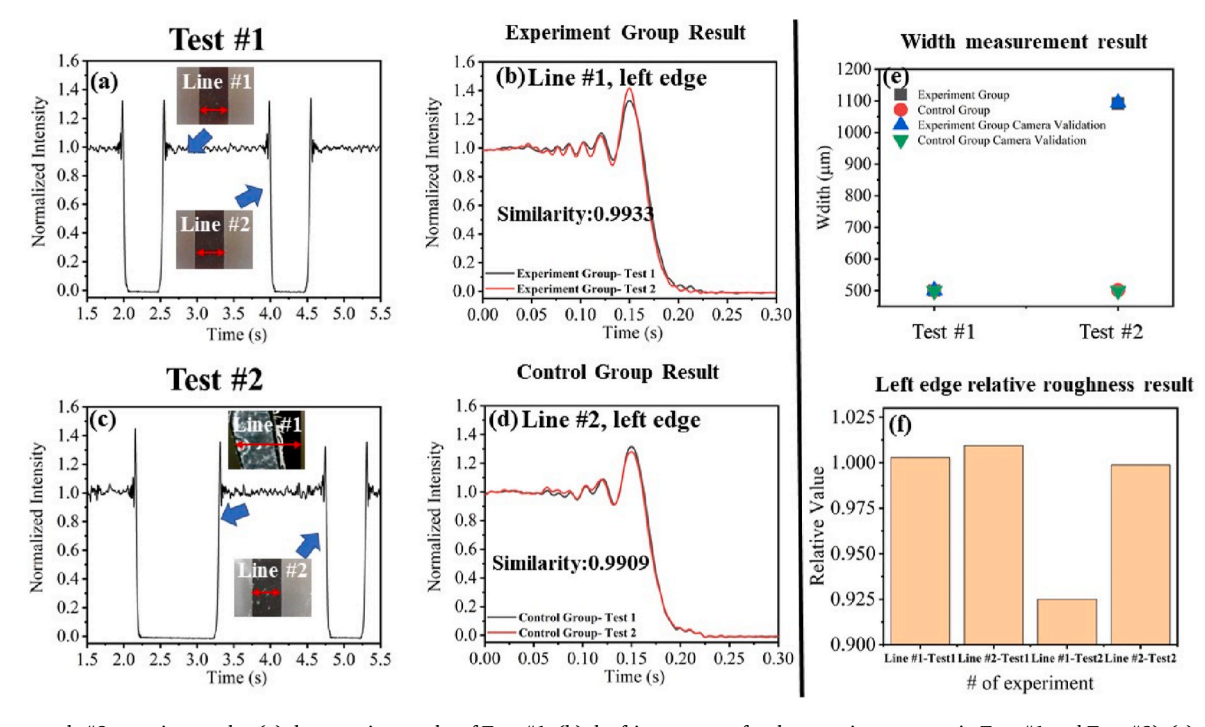


Fig. 5. Photomask #2 scanning results: (a) the scanning results of Test #1, (b) the fringe pattern for the experiment group in Test #1 and Test #2), (c) the scanning results of Test #2, (d) the fringe pattern for the control group in Test #1 and Test #2, (e) line width measurement result from the BSKEI method and validation by using an optical microscope, and (f) line edge roughness estimated by using the wavelet method.

This result indicates that BSKEI has the potential to diagnose the surface quality of the opening area.

(5) In Figs. 4f and 5f, when the defect was added to only one of two identical patterns onto the photomask, the relative value from the wavelet analysis method sensitively decreased compared with other no defect added groups. In the wavelet analysis method, all groups without the defect showed the relative value around 1, while the relative value from the group with defected edge decreased to 0.95. In the previous hypothesis, the additional film layer cut by a razor blade does not change the edge roughness

much. But the relative value for that group decreases to 0.925, which indicates that the edge roughness of that additional layer may not be as same as the edge roughness of the photomask pattern. Based on the simulation results and the experiment results, the wavelet analysis method for interferogram analysis shows its great potential for edge roughness diagnosis.

5. Conclusion and future works

This article introduces a new photomask inspection technology based on the BSKEI system and advanced fringe analysis methods. The geometrical optics based BSKEI model was developed, and simulated the interferogram analysis according to the NA of the objective lens. From the simulation results, it was confirmed that the use of objective lens improves the spatial frequency of the interferogram. With the objective lens added, the incident wave changes from a plane wave to a spherical wave, which decreases the averaging effect by the effective area of the photodiode and enhances the measurement resolution and sensitivity for the fringe analysis. In addition, the conventional fringe analysis method and wavelet-based feature extraction method were used to characterize the interferograms, and those methods were compared with the experimental data in terms of the interferogram analysis performance. As a result, the pattern width, pattern distance, LER, and arbitrary defects on the photomask were preliminarily inspected and characterized by BSKEI and interferogram analysis methods. As a result, it is expected that the BSKEI technology applies for photomask pattern dimension determination and edge roughness verification for highresolution photomask inspection systems. For future work, the 2-axis precision positioning system will be constructed to scan a whole photomask and to automatically reconstruct the pattern shapes and defects.

Author's contribution

All authors contributed equally to this work.

Data availability

The data that supports the findings of this study are available from the corresponding author upon reasonable request.

Declaration of competing interest

The authors declare that they have no known competing financial interests or personal relationships that could have appeared to influence the work reported in this paper.

Acknowledgment

This research has been supported by National Science Foundation (US) (CMMI #1855473). The photomasks were provided from the Oak Ridge National Laboratory (ORNL).

References

- Yoshioka Nobuyuki, Terasawa Tsuneo. Advanced mask inspection and metrology. AIP Conf Proc 2003;683:389.
- [2] Rothschild Mordechai. Projection optical lithography. Mater Today 2005;8(2): 18–24
- [3] Adam J, Berro Andrew J, Berglund Peter T, Jong Seung Kim Carmichael, Alexander Liddle J. Super-resolution optical measurement of nanoscale photoacid distribution in lithographic materials. ACS Nano 2012;6(11):9496–502. https://doi.org/ 10.1021/nn304285m.
- [4] Kamikubo Takashi, Ohnishi Takayuki, Hara Shigehiro, Anze Hirohito, Hattori Yoshiaki, Tamamushi Shuichi. Mask Process Correction (MPC) modeling and its application to EUV mask for Electron beam mask writer, EBM-7000. Proc SPIE 2010:26:12.
- [5] Sailer Hogler, Butschke Jörg. IMS chips photo mask technology, overview and classification, 2010. IMS Chips.
- [6] George Simi A, Naulleau Patrick P, Gullikson Eric M, Mochi Iacopo, Salmassi Farhad, Goldberg Kenneth A, Anderson Erik H. Replicated mask surface roughness effects on EUV lithographic patterning and line edge roughness. Proc. SPIE 7969, Extreme Ultraviolet (EUV) Lithography II 29 March 2011:79690E. https://doi.org/10.1117/12.881524.
- [7] George Simi A, Naulleau Patrick P, Mochi Iacopo, Salmassi Farhad, Gullikson Eric M, Goldberg Kenneth A, Anderson Erik H. Extreme ultraviolet mask substrate surface roughness effects on lithographic patterning. J Vac Sci Technol B 2010;28: C6E23. https://doi.org/10.1116/1.3502436.
- [8] Badger Karen D, Hibbs Michael, Rankin Jed, Seki Kazunori, Stobert Ian, Dechene dan J, Bleiman ben, Ghosal Mini, Broadbent William, Redding Vicent. Your worst nightmare – inspection of aggressive OPC on 14nm masks with emphasis on defect sensitivity and wafer defect print predictability. In: Proceedings. vol. 8880. Photomask Technology; 2013. 88800E. 2013.
- [9] Benschop Jos, Banine Vadim, Lok Sjoerd, Loopstra Erik. Extreme ultraviolet lithography: status and prospects. J Vac Sci Technol B: Microelectron Nanometer Struct Process Meas Phenom 2008;26:2204. https://doi.org/10.1116/1.3010737.
- [10] Chiang Charles, Jamil Kawa. Design for manufacturability and yield for nano-scale CMOS. Springer; 2007, ISBN 1-4020-5187-5. p. 237.
- [11] Kim Won Sun, Park Jin Hyung, Chung Dong Hoon, Jeon Chan Uk, Cho Han Ku, Hutchinson Trent, Lee Oscar, Huang William, Dayal Aditya. In: Proceedings, vol. 7488. Monterey, California, United States: Photomask Technology; 2009. 74882Q. https://doi.org/10.1117/12.830139Event: SPIE Photomask Technology. 2009, 2009.
- [12] Oh Sunghyun, Hwang DaeHo, Kim Inpyo, Kim Changreol, Tam Aviram, Ben Yishai Michael, Wolff Yulian. Proceedings. In: Photomask and next-generation lithography mask technology XVII, vol. 7748; 2010. p. 774827. https://doi.org/ 10.1117/12.869574Event: Photomask and NGL Mask Technology XVII. 2010, Yokohama, Japan.
- [13] Rajendran Rajeev, Mochi Iacopo, Helfenstein Patrick, Mohacsi Istvan, Redford Sophie, Mozzanica Aldo, Schmitt Bernd, Yoshitake Shushuke, Ekinci Yasin. Proceedings. In: Metrology, inspection, and process control for microlithography XXXI, vol. 10145; 2017. 101450N. https://doi.org/10.1117/ 12.2258379Event. SPIE Advanced Lithography, 2017, San Jose, California, United States.
- [14] Penley C, Bekka S. Characterization and reduction of pellicle degradation due to haze formation on leading edge technology photomasks. Surf Interface Anal 2017; 49(10):985–90.
- [15] Wang Zhiken, Lee ChaBum. Knife-edge interferogram analysis for corrosive wear propagation at sharp edge. Appl Opt 2021;60(5):1373–9.
- [16] Jeon Seongkyul, Stepanick Christopher K, Zolfaghari Abolfazl A. ChaBum Lee, Knife-edge interferometry for cutting tool wear monitoring. Precis Eng 2017;50: 354–60.
- [17] Jeon Seongkyul, Zolfaghari Abolfazl, Lee ChaBum. Dicing wheel wear monitoring technique utilizing edge diffraction effect. Measurement 2018;121:139–43.
- [18] Lee ChaBum, Lee Sun-Kyu, Tarbutton Joshua A. Novel design and sensitivity analysis of displacement measurement system utilizing knife edge diffraction for nanopositioning stages. Rev Sci Instrum 2014;85:095113.
- [19] Stavenga DG, van Hateren JH. Focusing by a high-power, low-Fresnel-number lens: the fly facet lens. J Opt Soc Am 1991;8:14–9.
- [20] Andén J, Mallat S. Deep scattering spectrum. IEEE Trans Signal Process 2014;62 (16):4114–28.
- [21] Mallat Stéphane. Group invariant scattering. Commun Pure Appl Math 2012;65 (10):1331–98.